THE UNIVERSITY of EDINBURGH

Edinburgh Research Explorer

Tuning the Wettability of Metal-Organic Frameworks via Defect Engineering for Efficient Oil/Water Separation

OPEN ACCESS

Tuning the Wettability of Metal-Organic Frameworks via Defect Engineering for Efficient Oil/Water Separation

Yi Huang [§,⊥,‡], Yang Jiao[§,‡],Ting Chen[⊥,‡], Yutao Gong[§,‡], Songcheng Wang[§], Yang Liu[§], David S. Sholl[§], Krista S. Walton[§,*]

[§]School of Chemical & Biomolecular Engineering, Georgia Institute of Technology, 311 Ferst Drive NW, Atlanta, Georgia 30332, United States. E-mail: krista.walton@chbe.gatech.edu.

[⊥]School of Engineering, Institute for Materials & Processes, The University of Edinburgh, Robert Stevenson Road, Edinburgh, EH9 3FB, United Kingdom.

KEYWORDS: Metal-organic frameworks, defect engineering, modulation synthesis, UiO−66, wettability, oil/water separation

‡These authors contributed equally

ABSTRACT

Zirconium-based metal-organic frameworks (MOFs) have attracted interest due to their chemical and thermal stability and structural tunability. In this work, we demonstrate the tuning of the wettability of UiO−66 structure via defect-engineering for efficient oil/water separation. UiO−66 crystals with controlled levels of missing-linker defects were synthesized using a modulation approach. As a result, the hydrophilicity of the defect-engineered UiO−66 (d−UiO−66) can be

varied. In addition, a thin layer of hydrophilic d−UiO−66 was successfully fabricated on a series of stainless steel meshes (d−UiO−66@mesh), which exhibited excellent superhydrophilic and underwater superoleophobic properties and displayed interesting separation performance for various oil/water mixtures.

INTRODUCTION

Metal-organic frameworks (MOFs) are a class of crystalline nanoporous materials constructed by self-assembly of metal-containing inorganic clusters and organic ligands.[1,2] They have attracted widespread interest because of the tunability of their porous lattice architectures.[3,4] The porous crystalline character of MOFs has made them promising for potential applications in various areas, including biology,[5] chemistry,[6] engineering,[7] and energy storage.[8] Although the majority of studies of MOFs regarded them as having ideal crystal structures,[9] synthesized MOFs always contain varieties of structural irregularities or defects.[10] These defects may be negligible in some cases. However, they can have a profound impact on both physical and chemical properties of MOFs and impact the overall performances in many applications.[11] Defects do not necessarily mean adverse influence. In fact, some regulated defects have been shown to positively influence the catalytic activity,[12−14] adsorption selectivity,[15,16] or decontamination capabilities[17,18] of various MOFs.[12−18]

Defect engineering, which refers to rational control over the structure, density, size or shape, and chemistry of defects, is an exciting concept for tuning specific properties desired in MOF materials.[19] This approach opens up opportunities for further manipulating MOFs performance in a wide range of targeted applications, such as CO_2 adsorption[20] and catalysis.[21] Approaches to the engineering control of defects in MOF structures include acid/base post-synthetic treatment[22] and

2

co-assembly of mixtures of ligands/ligand fragments strategy,[23] which is a more straightforward procedure as it creates defects in MOF structures in the course of crystallisation. Fundamentally, the latter strategy involves using isostructural mixed linkers[24] or heterostructural mixed linkers[25] to obtain mixed-linker MOFs. One well-studied example is the modulation approach, where monocarboxylate modulators (e.g. acetic, formic, or trifluoroacetic acid) are utilized as truncated linkers to promote defect formation in the Zr-terephthalate UiO−66.[26−28] These modulators can directly compete with the dicarboxylate linkers during the crystallisation process. As a result, the parent linkers in the ultimate framework are partially replaced by these modulators.[29] By applying the modulated synthesis route, a series of UiO−66 structures have been successfully prepared with different defect size, density and configuration in the structure. Interestingly, some defective UiO−66 crystals (d−UiO−66) have displayed significantly enhanced performance in a range of applications, such as catalysis,[21,30] gas adsorption,[31] and molecular-sieving.[32] However, very limited progress has been reported in using the above-mentioned defect MOF crystals in liquid separations.

Generation of oily wastewater from domestic activities, petrochemical industries, and oil spills has become a severe threat to the global ecosystem and human health.[33] Water remediation is, therefore, of significant importance to the modern society.[34] In recent years, the development of scalable and energy-saving techniques, particularly those involving novel advanced separation materials, for the efficient treatment of oil-contaminated water has attracted extensive attention. A new category of biomimetic materials with unique wetting properties became an effective and facile approach to achieve efficient oil/water separation.[35−37] For example, inspired by the unique underwater oil-repellent properties of fish scales, materials with underwater superoleophobic surfaces were prepared and successfully applied to oily wastewater treatment.[38−40]

In this work, we demonstrate the tuning of the hydrophilicity of MOF crystals via defect engineering for efficient oil/water separations. The Zr-based MOF UiO−66 was employed in this study due to its hydrothermal and chemical stability.[41−43] A modulation-based approach was applied to generate missing linker or cluster defects in the UiO−66 framework.[26,31] The resulting defect-engineered UiO−66 (d−UiO−66) showed enhanced hydrophilicity compared to the parent UiO−66. The defective, hydrophilic d−UiO−66 was then successfully coated onto a series of polydopamine (PDA) coated stainless steel meshes.[44] The d−UiO−66 mesh films exhibited interesting superhydrophilic and underwater superoleophobic properties and achieved efficient oil removal from aqueous solutions. Moreover, they showed excellent structural stability after either 3-month soaking in water or 50 cycles of oil/water separation.

EXPERIMENTAL SECTION

Modulated synthesis of UiO−66s (d−UiO−66)

Parent "defect-free" UiO−66 crystals were prepared from a clear solution with a molar ratio of ZrCl$_4$ (Sigma-Aldrich, ≥99.9% trace metals basis): H$_2$BDC (BDC = benzene-1,4-dicarboxylate, Sigma-Aldrich, 98%): DMF (Sigma-Aldrich, anhydrous, 99.8%) = 1:1:500 (or 0.159 g: 0.114 g: 24.9 g according to the weight ratio).[45] For the preparation of defective UiO−66 crystals (d−UiO−66), acetic acid (Sigma-Aldrich, ≥99%) was added as the modulator. The following recipes were used: ZrCl$_4$: H$_2$BDC: DMF: Acid (acetic acid) = 1: 1: 500: x (x = 15, 30, or 70 in terms of molar ratio). The mixture solution was transferred to a stainless steel autoclave and then heated to 150 °C for 24 h. The product was washed with fresh DMF by repeated centrifugation and then dried in the oven overnight at 80 °C. The defective UiO−66 samples synthesized in this work were denoted as d−UiO−66_1 (x = 15), d−UiO−66_2 (x = 30), and d−UiO−66_3 (x = 70),

respectively. Parent UiO−66 was prepared with a molar ratio of 1 ZrCl₄: 1 H₂BDC: 500 DMF. The mixture was heated to 200 °C and kept for 48 h in order to complete the crystallization. The product was washed with fresh DMF repeatedly and then dried at 80 ℃ overnight. All samples were then stored in a drying desiccator cabinet before use.

Fabrication of d−UiO−66 coated mesh

A series of stainless steel meshes (US mesh size 50, 150, 270, 325, 400, 500 and 600) were ordered from Direct Metals Company, LLC and then cleaned adequately in ethanol and water before use. In a typical synthesis of UiO−66 on mesh 400 (aperture size 37 μm), a piece of pre-cleaned mesh was first coated with a thin layer of polydopamine (PDA) by following the procedures as described in previous work.[44] The PDA-coated mesh was then placed vertically in a 45 mL Teflon-lined stainless steel autoclave and immersed into a 25 mL synthesis solution with a molar ratio of ZrCl₄: H₂BDC: DMF: Acid (acetic acid) = 1: 1: 500: y (y = 15, 30, or 70) and then heated to 150 °C for 6 h, 24 h, and 48 h. The as-synthesized stainless steel mesh film was then washed with DMF at least 3 times and denoted as d−UiO−66@mesh number.

Oil-water separation experiments

The UiO−66@mesh films were placed securely in a homemade separation device (Figure S1) and fixed with two foldback clips in the middle. A mixture of water and oil with a volume ratio of 50:50 was poured directly onto the mesh surface. In this study, n-hexane (Sigma-Aldrich, anhydrous, 95%), n-decane (Sigma-Aldrich, anhydrous, ≥99%), Soybean oil (Princes Ltd), cyclohexane (Sigma-Aldrich, anhydrous, 99.5%), chloroform (Sigma-Aldrich, ≥99.5%) and n-heptane (Sigma-Aldrich, ≥99%) were ordered and used without further purification. The oils were

dyed with oil red O for clear observation, and the permeated liquid was collected in a beaker with a scale placed at the bottom. The whole separation process was driven solely by gravity without applying external pressure.

Characterization

Powder X-ray diffraction (PXRD) patterns were recorded on a PANalytical X-ray diffractometer with a Cu Kα X-ray source ($\lambda = 1.5418$ Å). PXRD diffractograms were collected in a 2θ range of $5 - 50°$ under ambient conditions. Scanning electron microscopy (SEM) images were taken on a Zeiss Ultra60 Field Emission Scanning Electron Microscope. Nitrogen adsorption measurements at 77 K were performed using a Quadrasorb system from Quantachrome Instruments. Specific surface areas of the samples were determined using the BET model with the relative pressure (P/P_0) in the range of $0.005 - 0.03$. Water adsorption isotherms at 298 K and 1 bar were obtained using an IGA−003 microbalance from Hiden Isochema. Dry air was employed as the carrier gas, and the relative humidity (RH) was controlled by adjusting the ratio of the saturated air and the dry air through mass flow controllers. Thermogravimetric analysis (TGA) of the samples were performed using ETZSCH STA 449 F1 Jupiter instrument. The curves were obtained under helium with a flow rate of 20 mL min^{-1}, a temperature range of $25 - 800$ °C, and a heating rate of 5 °C/min. Contact angle measurements were carried out using a ramé-hart goniometer (model−250). A 22 gauge needle was used to squeeze a drop of water or oil onto the flat mesh surface, and the images were captured within one minute. UiO−66 pellets were prepared by adding ~0.2 g of the powder into the Clarke Strong-Arm and pressing the powder under a pressure of ~1000 psi for 1 minute to form a pellet.

Multiple UiO−66 structures were optimized with spatially-periodic Density Functional Theory (DFT) calculations (more details in Supporting Information). Zero-loading heats of adsorption for H_2O in defect-free and defective UiO–66 were simulated using classical force fields with Grand Canonical Monte Carlo (GCMC) simulations (more details in Supporting Information).

RESULTS AND DISCUSSION

Modulated synthesis of UiO−66 crystals and their hydrophilicity

UiO−66 crystals with different densities of defects were prepared following a modulated synthesis route by using acetic acid as the modulator. A schematic model of the defect formation process in UiO−66 framework is presented in Figure 1a. The UiO−66 structures shown in this figure were optimized by Density Functional Theory calculations with periodic models performed in the Vienna Ab initio Simulation Package (VASP) (Supporting Information). In ideal UiO−66 crystals, each Zr metal center is coordinated by 12 organic linkers (Figure 1a, top-left structure).[32] In the synthesized UiO−66 crystals, missing-linker defects inevitably exist inside the framework. This has been unambiguously confirmed previously with high-quality neutron diffraction measurements.[32] For some MOFs, a missing linker would possibly lead to pore collapse issues inside the crystal structure.[32] UiO−66 is more tolerant to the missing-linker defects due to its high metal-ligand connectivity[26]. Therefore, the missing-linkers in the UiO−66 structure can result in linker vacancies without significantly disrupting the original framework topology (Figure 1a, top-right structure). Missing-linker defect formation in UiO−66 can be promoted by introducing the acetic acid modulator because the acetic acid would act as the defect-compensating ligand to compete with the linkers. In the resulting defective crystal framework, linkers would be partially

substituted by the deprotonated acetic acid modulator (acetate), while positive charges on the open metal sites

would be balanced by terminal groups, such as −OH groups.[46] It has also been reported that the linker vacancies (thus the open metal sites) can be systematically varied by varying the acetic acid to carboxylate ligand ratio in the synthesis solution. The defectivity of the crystals was found to increase systematically and dramatically as the concentration and/or acidity of the modulator was increased.[26] This suggests that the density of –OH groups in UiO−66, and therefore, its hydrophilicity can be tuned via the modulation synthesis.
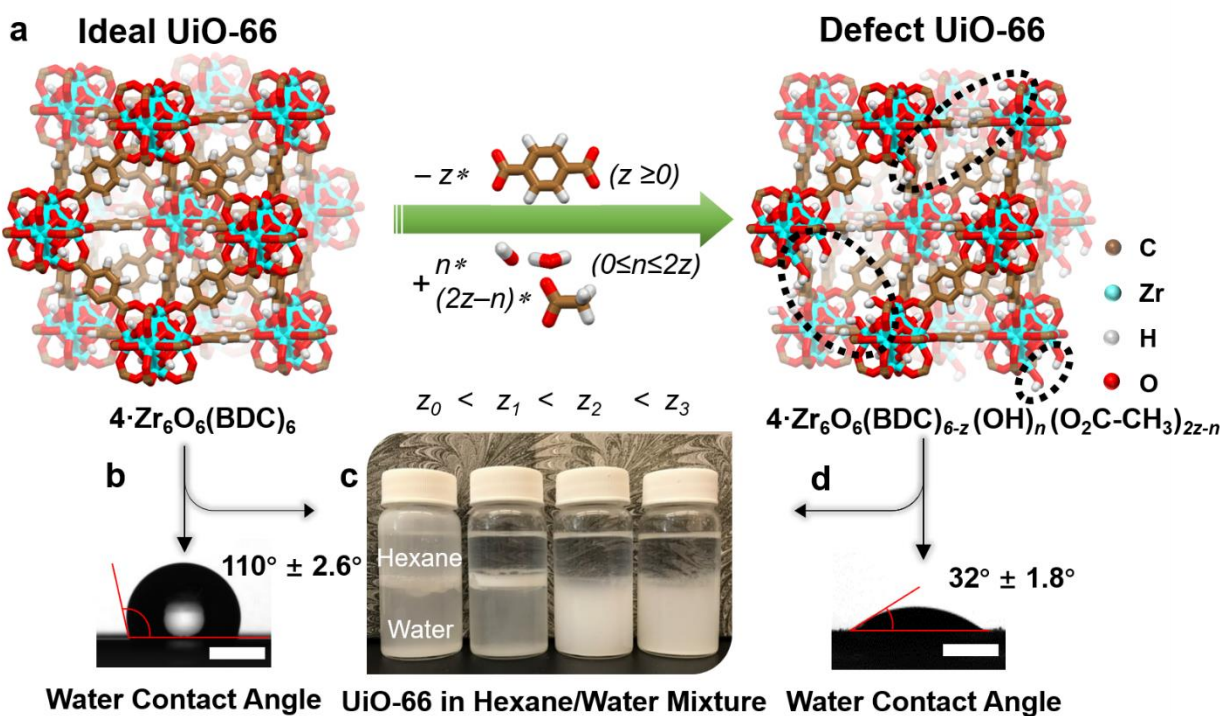
Figure 1. (a) Illustration depicting missing-linker defect formation in the UiO−66 structure. (b) Water contact angle of the parent UiO−66. Scale bar, 1 mm. (c) Dispersibility of UiO−66 samples synthesized with different concentrations of acetic acid in a immiscible hexane/water mixture (40/60, v/v. (d) Water contact angle of the d−UiO−66_2. Scale bar, 1 mm. z and n denote the number of missing linkers and capping water or –OH groups, respectively.

To study their wetting properties, parent UiO−66 with minimal defects and its defective analogues (d−UiO−66s) were prepared via modulation synthesis. As-synthesized powders were firstly dispersed separately in a 40/60 (v/v) hexane/water mixture (Figure 1c). The parent UiO−66 appeared in both oil and aqueous phases as well as at the oil-water interface (Figure 1c, first vial from the left). When a small amount of acetic acid ($n_{\text{Acetic acid}}/n_{\text{Zr}}$ is 15) was used in the modulation synthesis, the majority of the resulting crystals were strongly attracted to oil-water interfaces, forming a thin layer of metastable oil and water emulsions (Figure 1c, second vial from the left). The UiO−66 crystals with further increased framework defect densities ($n_{\text{Acetic acid}}/n_{\text{Zr}} \geq 30$), appeared only in the bottom aqueous phase and exhibited excellent dispersibility (Figure 1c, third and fourth vials from the left), indicating a further increase in hydrophilicity.

The surface wettability of defective UiO−66 pellets was also analysed using a contact angle goniometer. When the molar synthesis ratio, $n_{\text{Acetic acid}}/n_{\text{Zr}}$ is 30, the UiO−66 sample was highly hydrophilic in air and showed a water contact angle of $32° \pm 1.8°$ (Figure 1d) and a fast water diffusion rate in less than 3s (Video S1). For less defective UiO−66 sample prepared with a $n_{\text{Acetic acid}}/n_{\text{Zr}}$ of 15, the water droplet stayed statically on the pellet surface and remained almost unchanged in 1 min (Video S2). The above results again indicate that the hydrophilicity of UiO−66 can be adjusted by altering the concentration of modulators in the synthesis solution.
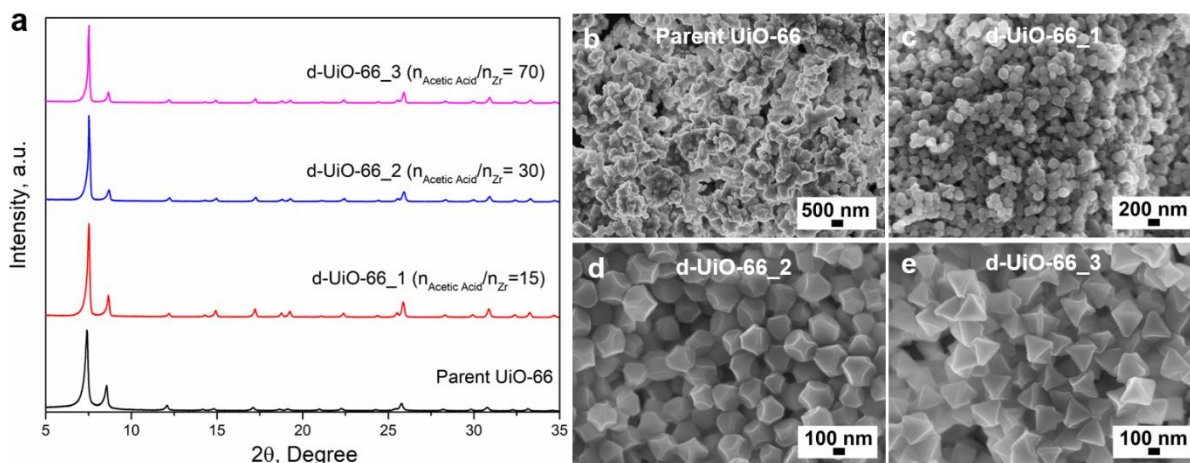
Figure 2. (a) PXRD patterns and (b) − (e) SEM images of UiO−66 samples synthesized with different amounts of acetic acid.

The influence of the acetic acid on the crystallization was then studied by PXRD patterns (Figure 2a). All samples showed characteristic UiO−66 diffraction patterns without impure phases.[26] The PXRD peaks of d−UiO−66 samples showed slightly narrower full width at half maximum (FWHM) values compared to the reference (parent UiO−66), with the FWHM values decreased by ~25%, ~39% and ~58% respectively when 15, 30 and 70 equivalents of acetic acid were added, suggesting larger defective crystals were formed. The size change was again confirmed by SEM studies. As shown in Figure 2b, the parent UiO−66 consisted of intergrown aggregates of small spherical particles with an average size of ~200 nm. After the addition of 15 equivalents of acetic acid ($n_{Acetic\ acid}/n_{Zr}$ = 15), single-crystalline UiO−66 nanocrystals with an average size of ~220 nm were formed (Figure 2c). Further enhancing the $n_{Acetic\ acid}/n_{Zr}$ ratio to 30 (d−UiO−66_2) and 70 (d−UiO−66_3) in the synthesis solution led to the crystallization of uniform UiO−66 crystals with a well-developed octahedral shape. The average crystal size was further increased to ~300 nm and ~400 nm for d−UiO−66_2 and d−UiO−66_3 samples, respectively (Figure 2d and 2e). These results indicated that the size and morphology of UiO−66 could be regulated by varying the amount of acetic acid in the synthesis solution. During the modulation synthesis, the competition between

acetate and the deprotonated linker (BDC^{2-}) inhibited crystal nucleation and thus fewer nuclei were formed.[26] On the other hand, higher acetic acid concentration favors the crystal growth leading to the formation of crystals with high crystallinity.[27] As a result, the morphology of the UiO−66 crystals gradually changes from small intergrown cubes to larger, single octahedral when increasing the acetic acid concentration.

The number of the missing linker per Zr_6 formula unit in the defective UiO−66 analogues prepared with different molar equivalents of the acetic acid modulator was calculated based on their TGA-DSC data using the method reported previously[26]. An example of the missing linker calculation using the TGA-DSC data is shown in Figure 3a. The weight loss observed over the temperature range of 25 °C-100 °C in the TGA curve is attributed to the desorption of adsorbed water in the structure. Then the loss of the monocarboxylate ligands (acetic acid) and the dehydroxylation of the Zr_6 cornerstones occur over the temperature range of 200 °C-395 °C, which is in good agreement with previous studies.[26,43]
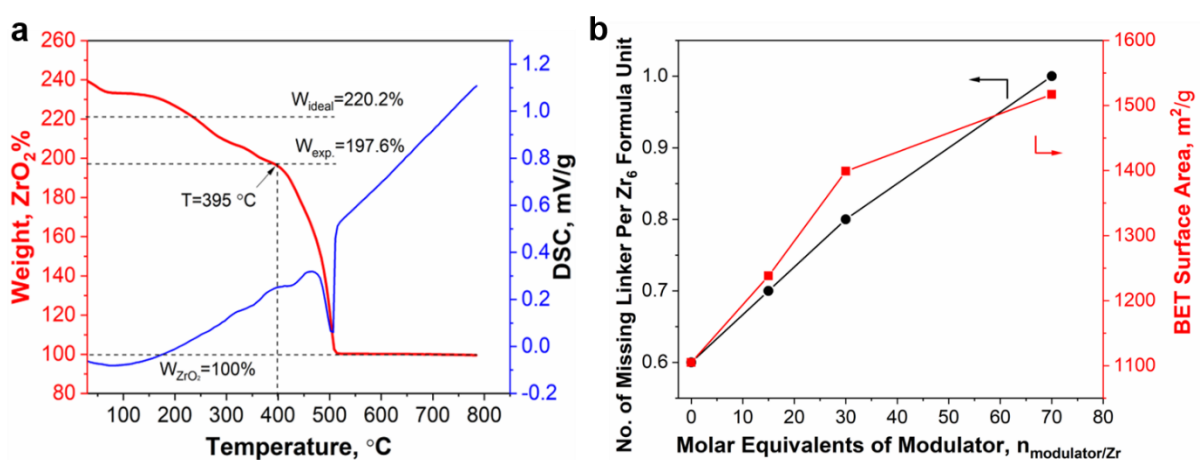

Figure 3. (a) An example of the missing linker calculation using TGA-DSC data for d−UiO−66_3 sample. (b) Effect of molar equivalent of the modulator on the number of missing linkers and BET surface areas in UiO−66 samples

Table 1. BET surface areas before and after hydrothermal stability tests and water adsorption loadings at 90% relative humidity

Samples	Modulator Amount[1] ($n_{AA/Zr}$)	Yield[2] (%)	BET Surface Area (m²/g) Before	After	Loss of BET	Water Loading[3] (mmol/g)
			3-month water soaking test		(%)	
UiO−66	0	~60	1105	1083	2.0	18.9
d−UiO−66_1	15	~55	1238	1206	2.6	24.8
d−UiO−66_2	30	~52	1399	1355	3.2	30.0
d−UiO−66_3	70	~35	1517	1327	12.5	29.0

Note: 1, $n_{AA/Zr}$ denotes the mole ratio of acetic acid to Zr. 2, The yield of all samples was estimated with respect to the mass of zirconium salt. 3, Water loading of the samples at 90% relative humidity (RH).

After that, the decomposition of the framework begins from 395 ℃ to 500 ℃, which includes the complete removal of the BDC linkers. The number of missing linker per Zr_6 formula unit was calculated using the method reported by Shearer et. al.[26] (refer to Supporting Information for more details). As shown in Figure 3b, the number of missing linkers was significantly increased with the increasing amount of acetic acid modulator. The calculated number of missing linkers per Zr_6 centre increased from ~0.7 for d−UiO−66_1 to ~1.0 for d−UiO−66_3 (see also Table S1,). Their BET surface areas increased correspondingly (Table 1). The parent UiO−66 (obtained with a yield of ~60%) has a typical BET surface area of 1105 m² g⁻¹, which is consistent with the value reported by Sholl et al.[47] The d−UiO−66_1 sample (obtained with a yield of ~55%) shows an increased surface area of 1238 m² g⁻¹ due to the formation of missing-linker defects in the UiO−66 framework. When the amount of acetic acid was increased to 30 equivalents, BET surface area of the obtained d−UiO−66_2 sample (with the yield slightly decreased to ~52%) further increased to 1399 m² g⁻¹, indicating higher defectivity of the UiO−66 framework. The last d−UiO−66_3 sample

prepared with 70 equivalents of acetic acid showed a BET surface area over 1500 m^2 g^{-1}, but with a low yield of ~35%. This is because comparing to d−UiO−66_1, a higher concentration of acetate exists in d−UiO−66_3 to compete with the linkers in the course of crystallization.[26−28] Thus, the number of acetic acid modulator remaining compensated in d−UiO−66_3 framework increases, resulting in more linker deficiencies in the final product.

To understand how the number of missing linkers or missing linker vacancies influence the hydrophilicity of the UiO−66 framework, molecular simulation of the parent and d−UiO−66 samples was conducted to estimate the heats of adsorption of water at low loading (ΔH_{H_2O}) in the framework. Zero-loading heats of adsorption for H_2O in defect-free, CH_3COO^- capped defective, and H_2O/OH^- capped defective UiO−66 at room temperature were calculated using Grand Canonical Monte Carlo (GCMC) simulations in RASPA, and the results were shown in Table 2 (refer to Supporting Information for more details on density functional theory (DFT) calculations and molecular simulations).

Table 2. Amount of missing linkers in parent and defective UiO−66 samples and their simulated water heat of adsorption

Materials	The number of missing linker per Zr$_6$ Centre	ΔH_{H_2O}, kJ/mol, 298K
UiO−66	0	−13
d−UiO−66_AA	0.5 ~ 1.5	−14 ~ −15
d−UiO−66_OH	0.5 ~ 1.5	−46 ~ −47
d−UiO−66_1	0.7	−14 ~ −47
d−UiO−66_2	0.8	−14 ~ −47
d−UiO−66_3	1.0	−14 ~ −47

Note: d−UiO−66_AA and d−UiO−66_OH denote CH_3COO^- capping and H_2O/OH^- capping d−UiO−66s, respectively.

In Table 2, the ideal UiO−66 sample showed a very weak heat of adsorption of water, −13 kJ/mol at 25 °C, suggesting that the UiO−66 framework was intrinsically hydrophobic. Further increasing the number of missing linkers unavoidably yield more linker vacancies in the unit cell. As discussed above, the missing-linker defect could be substituted by either the deprotonated acetic acid modulator (acetate) or hydrophilic terminal groups, such as −OH groups. According to GCMC calculations, the ΔH_{H2O} of UiO−66 remained almost constant at −14 kJ/mol when all missing linker vacancies were compensated by acetate groups On the other hand, if only water or –OH groups were terminated in the missing linker defects, the calculated value of ΔH_{H2O} was sharply decreased to −46 kJ/mol, indicating that the framework became highly hydrophilic in nature. Indeed, the more defective UiO−66 structures displayed enhanced water adsorption performance under a series of test relative humidity (RH) at room temperature (25 °C). As shown in Figure 4, all defective UiO−66 samples exhibited much higher water uptake as compared to the parent UiO−66 (see also Table S2).
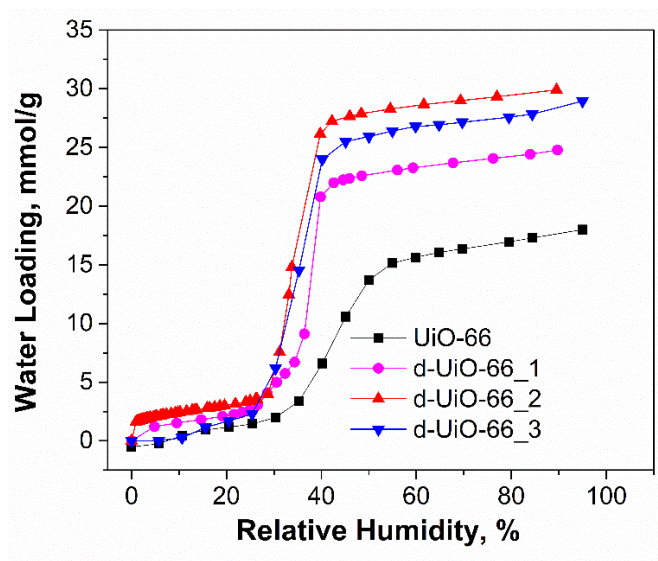

Figure 4. Water adsorption behaviour of parent and defect UiO−66 samples under different relative humidity at room temperature.

For instance, at 90% RH, a steady increase in total water loading was observed for the parent UiO−66 (18.9 mmol/g), d−UiO−66_1 (24.8 mmol/g), d−UiO−66_3 (28.95 mmol/g) and d−UiO−66_2 (30.0 mmol/g) (see also Table 1). These results further suggest that the defective UiO−66 samples possess stronger affinities for water than the parent UiO−66.

In this work, when a high modulator ratio (e.g., 30 and 70) was used, the final d−UiO−66 samples showed greatly improved hydrophilicity which implies water molecules or –OH groups are more preferably compensated in the missing linker defects even at conditions with a high acetic acid concentration. Both d−UiO−66_2 and d−UiO−66_3 were found to be highly hydrophilic according to their water adsorption and surface contact angle measurements (Figure 1d, Table 1 and Figure 4). Considering a relatively low yield of the latter sample (~35%), hydrophilic d−UiO−66_2 which possessed a much higher yield rate (~52%) and water uptake (29.9 mmol/g) was chosen as a suitable candidate for the following hydrothermal stability tests and liquid separation studies.

Hydrothermal stability of hydrophilic d−UiO−66 samples

Hydrothermal stability of the separation materials has always been one of the critical parameters which could affect the long-term separation performance. It has been reported that UiO−66 is one of the few MOFs which are thermally stable up to 500 °C.[26–27] However, its hydrothermal stability has not been fully studied. We tested the hydrothermal stability of the synthesized UiO−66 samples by soaking them in deionised water for an extended period of 3 months at room temperature (25 °C). N_2 sorption and PXRD measurements were used to monitor the change of their structures. BET surface areas of the synthesized UiO−66 samples before and after the stability tests were summarized in Table 1. After soaking in water, the BET surface area of the parent UiO−66 was

reduced by only 2.0%, indicating the parent UiO−66 structure showed outstanding stability in water at room temperature. For the d−UiO−66_1 and d−UiO−66_2 samples, the loss of their BET surface areas slightly increased to 2.6% and 3.2%, respectively, confirming that these two defective UiO−66 analogues still possessed satisfactory hydrothermal stability at room temperature. A more significant BET surface area loss of ~12.5% was found for the d−UiO−66_3 sample implying the higher framework defectivity could lead to a compromise of its hydrothermal stability. However, according to PXRD results, all samples before and after the stability tests showed similar representative UiO−66 diffraction peaks, which matched well with the simulated pattern (Figure S2). These results strongly suggest that all samples retained almost full crystalline integrities after 3-month soaking in water and still exhibited excellent stability.

Fabrication of superhydrophilic d−UiO−66 coated meshes

The hydrophilicity and stability of the as-synthesized d−UiO−66s make them a potential candidate for long-term stable oil/water separations. We prepared d−UiO−66@mesh materials on a series of stainless steel meshes with different aperture sizes via a simple dip-coating process. An illustration of the 2-step fabrication process is shown in Figure 5a.
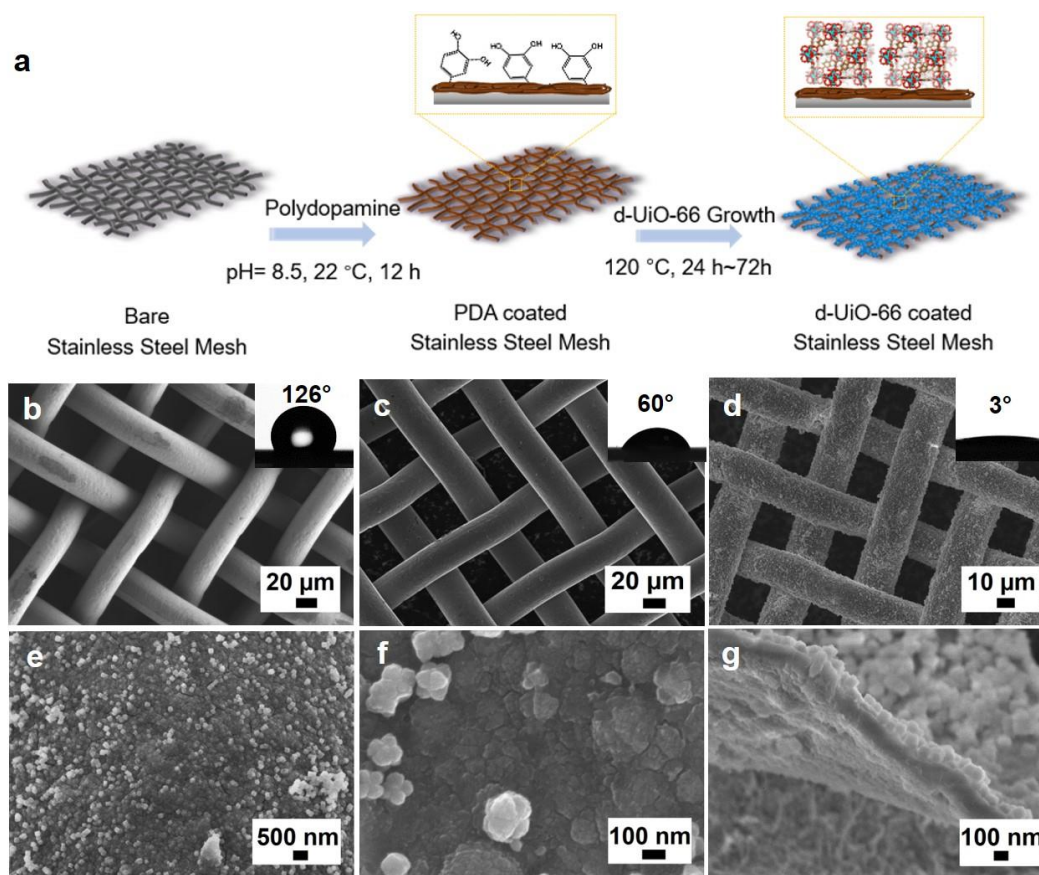
Figure 5. (a) Schematic illustration for the fabrication process of the d−UiO−66@mesh; and (b) − (g) SEM images of d−UiO−66_2 @mesh 400 samples at different stages of the fabrication process.

d−UiO−66_2 was chosen as a representative for the growth. In the first step, a clean mesh was coated with a thin layer of polydopamine (PDA) by immersing the mesh into a dopamine aqueous solution under alkaline condition (pH = 8.5) for 12 h. With a thin layer of PDA serving as the adhesive agent, the mesh surface became highly hydrophilic.[44] The PDA-coated mesh was then immersed in the d−UiO−66 synthesis solution for the growth of d−UiO−66 on the mesh surface. Figure 5b shows the SEM image of a bare stainless steel mesh (US size 400) with a smooth surface. However, the pristine mesh is hydrophobic in air as a water contact angle as high as 126° was observed (Figure 5b, inset). After dip-coating in polydopamine solution, the PDA-coated mesh showed no noticeable change on the surface as presented in Figure 5c, but its water contact angle

17

decreased dramatically to ~60° (Figure 5c, inset). Figure 5d and 5e show the original smooth mesh surface was completely covered by a dense layer of d−UiO−66_2 crystals and the d−UiO−66_2@mesh 400 became superhydrophilic with a water contact angle smaller than 5°. High-magnification SEM images (Figure 5f and 5g) further revealed that the dense layer (~ 350 nm) was composed of abundant intergrown d−UiO−66_2 crystals, forming a continuous nanoscale rough surface. Without the PDA coating, only a scattered coverage of crystals was found on the d−UiO−66_2@mesh surface (Figure S3 a − c). In this situation, instead of forming a continuous layer on the mesh surface, the UiO−66 crystals tend to be agglomerated into numbers of isolated islands. The above results indicate that the PDA layer helped promote uniform nucleation and crystal growth on the mesh surface. d−UiO−66_3@meshes 400 were also prepared and studied. According to the SEM results (Figure S3 d − f), further increasing the amount of the modulator had no noticeable change on the crystal coverage and uniformity, except the d−UiO−66_3 crystals were less intergrown on the mesh surface. Considering the low yield rate of d−UiO−66_3 and incomplete crystal intergrowth on the mesh surface, d−UiO−66_2 was used for further testing of d−UiO−66@meshes.

Wettability of d−UiO−66_2@meshes

The wetting properties of stainless steel meshes with different mesh number before and after coating with UiO−66 were systematically characterized using contact angle measurements. As presented in Figure 6, all the bare meshes exhibited hydrophobic properties in air with a water contact angle in the range of 116° - 127°. After coating by a thin layer of d−UiO−66_2, the mesh surfaces were superhydrophilic in air. Most mesh samples showed an in-air water contact angle lower than ~5°.

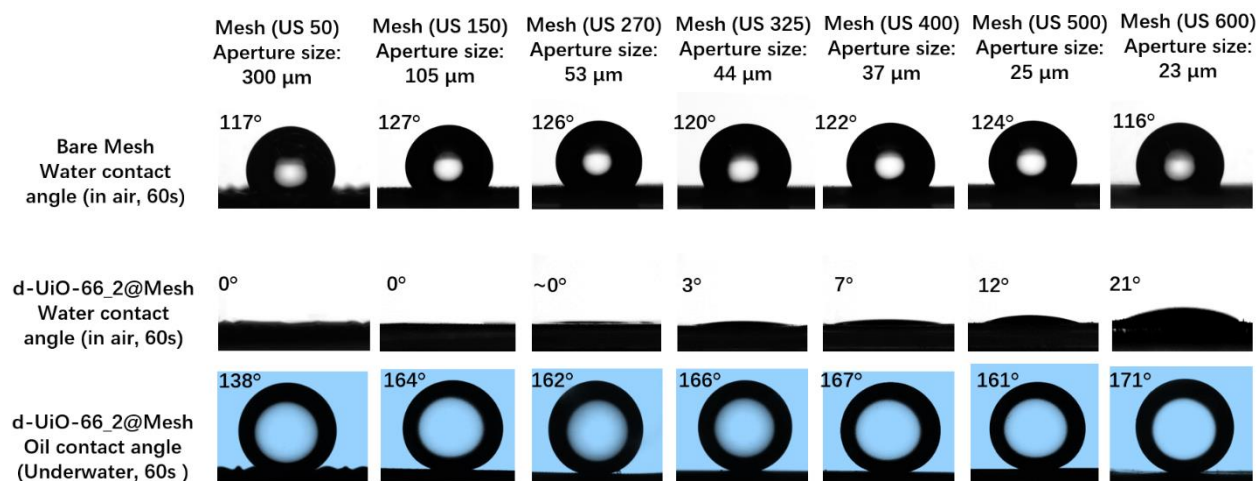| Mesh (US 50) Aperture size: 300 μm | Mesh (US 150) Aperture size: 105 μm | Mesh (US 270) Aperture size: 53 μm | Mesh (US 325) Aperture size: 44 μm | Mesh (US 400) Aperture size: 37 μm | Mesh (US 500) Aperture size: 25 μm | Mesh (US 600) Aperture size: 23 μm |

Figure 6. Water contact angle of bare meshes (top row), d−UiO−66_2@meshes (middle row), and underwater oil contact angle (bottom row) of d−UiO−66_2@meshes.

When the mesh pore size further decreased to < 40 μm (e.g., US meshes 400, 500 and 600), the water contact angle (measured at 60 s) was slightly increased as water permeation through the mesh with a smaller pore was slower, therefore more water remains on top forming a larger contact angle. Underwater wetting properties of all meshes were studied by immersing these meshes in water and performing underwater oil contact measurements. Trimethylolpropane trimethacrylate (TMTA) which has a density of 1.06 g/mL was employed as the representative heavy oil. All the meshes displayed excellent underwater superoleophobicity, with an oil contact angle higher than 160° except d−UiO−66_2@mesh 50. Such superhydrophilic and superoleophobic surface wetting properties make the d−UiO−66@ meshes interesting for oil/water separation.

Oil/water separation performance

Gravity-driven oil/water separation performance was examined using a homemade setup as shown in Figure 7a. The mesh samples were clamped between two identical plastic tubes with two foldback clips. Then, immiscible oil/water mixtures with a volume ratio of 50:50 and oil phase dyed with a red colour were poured onto the mesh surface.
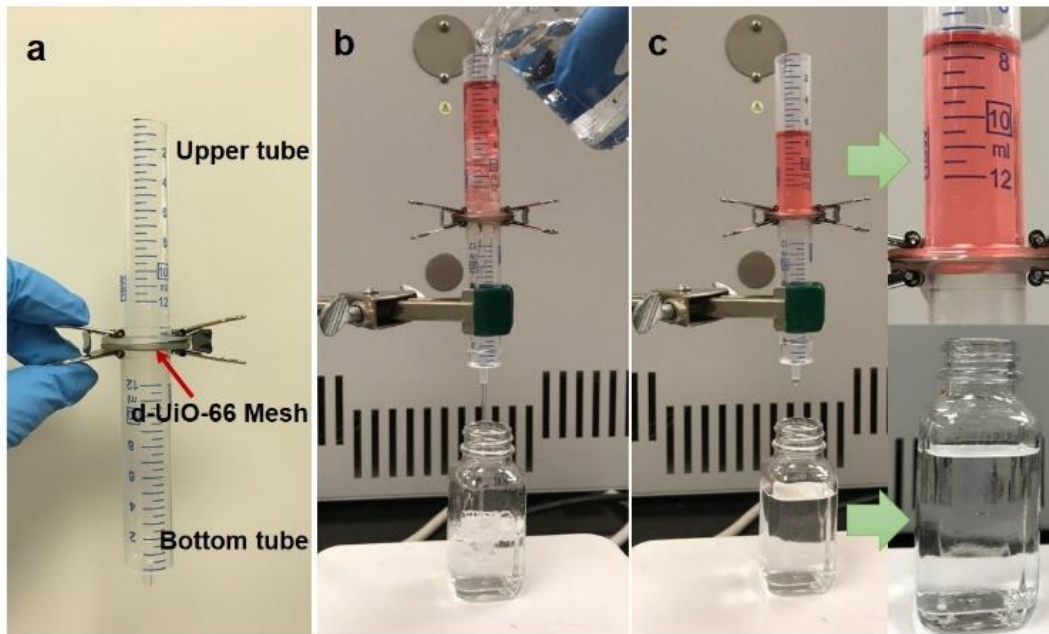
Figure 7. Oil/water separation performance of d−UiO−66_2@meshes-400. (a) A photo of the homemade device. (b) A mixture of n-hexane and water (50/50, v/v) was poured into the plastic tube. (c) Water permeate through the mesh under gravity, but n-hexane was completely rejected above the mesh.

Figure 7b and 7c show a photo of the oil (n-hexane)/water separation on d−UiO−66_2@mesh 400 at the early beginning and the end of the separation experiment, respectively. Compared to the bare stainless steel mesh, PDA coated mesh and UiO−66@mesh 400 which had no selective oil or water permeation (Video S3, S4 and S5), the d−UiO−66_2 coated meshes only allowed the permeation of water while completely rejected the oil (Video S6). Moreover, the oil remained above the mesh even after strong flushing with water from the top for several times, suggesting excellent and stable oil/water separation performance was achieved.

The performance was also measured on d−UiO−66@meshes with different aperture size. The permeate flux (F) was calculated using equation (3):

$$F = V/S \cdot t \tag{3}$$

where V is the total volume of the filtrate (L), S is the effective filtration area of the mesh (m^2), and t is the filtration time (s).

The intrusion pressure was determined by measuring the maximum height of the oil column that the mesh sustained, and was calculated using the following equation:

$$\Delta P = \rho g h_{max} \qquad (4)$$

where ΔP is the intrusion pressure, ρ is the density of the oil, g is the gravity acceleration, and h_{max} is the maximum height of the oil column that stayed above the mesh. As shown in Figure 8a, the permeate flux of the d−UiO−66_2@meshes increased with the increase of the mesh aperture size, while an opposite trend was observed for the intrusion pressure. According to the measurements, when the aperture size of the mesh was in the range of 25 μm to 45 μm, the d−UiO−66_2@meshes has the optimal performance with the flux ranging from 30 L m^{-2} s^{-1} to 50 L m^{-2} s^{-1} and the intrusion pressure ranging from 750 Pa to 825 Pa (see also Table S3).
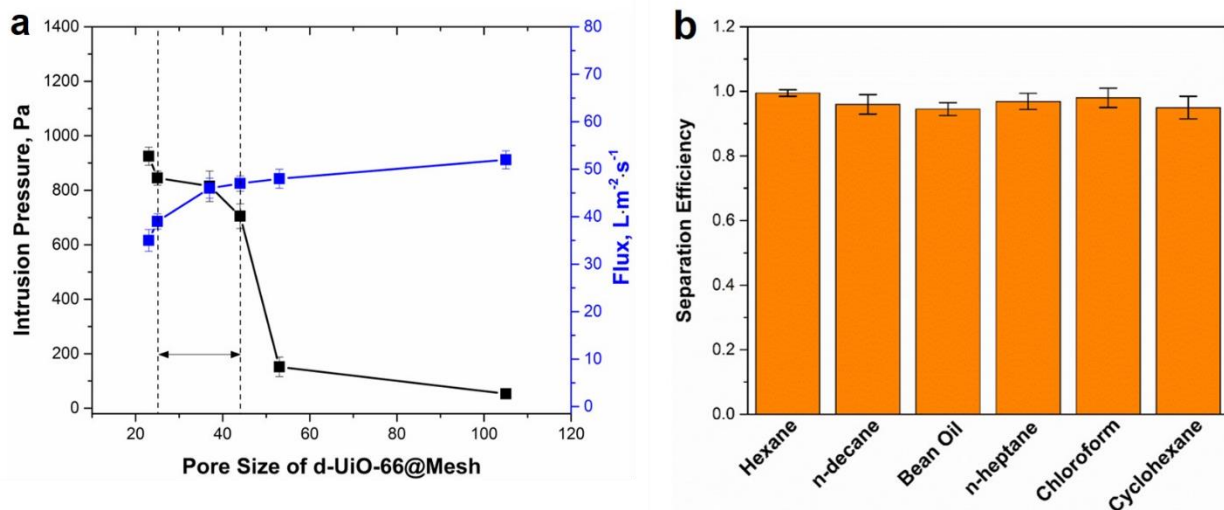

Figure 8. (a) Influence of pore size on the flux and intrusion pressure of the d−UiO−66_2@mesh. (b) The separation efficiencies of the d−UiO−66_2@mesh for various oils in terms of oil rejection coefficient.

Various oil/water mixtures were prepared for the oil rejection tests on a series of d−UiO−66@meshes 400. The separation efficiency (R) was calculated using equation (5):

$$R = \left(1 - \frac{c_p}{c_0}\right) \times 100\% \qquad (5)$$

where C_0 is the initial oil content in the feed oil/water mixture, and C_p is the oil content in the collected filtrate. Our results revealed that the d−UiO−66_2@meshes 400 exhibited excellent separation performance among all tested oils with a separation efficiency, R, higher than 99.9% (Figure 8b, see also Table S4), underscoring the d−UiO−66@meshes 400 obtained in this work are very promising for highly-efficient separation of various oil/water mixtures.

Recyclability and stability of d−UiO−66@meshes

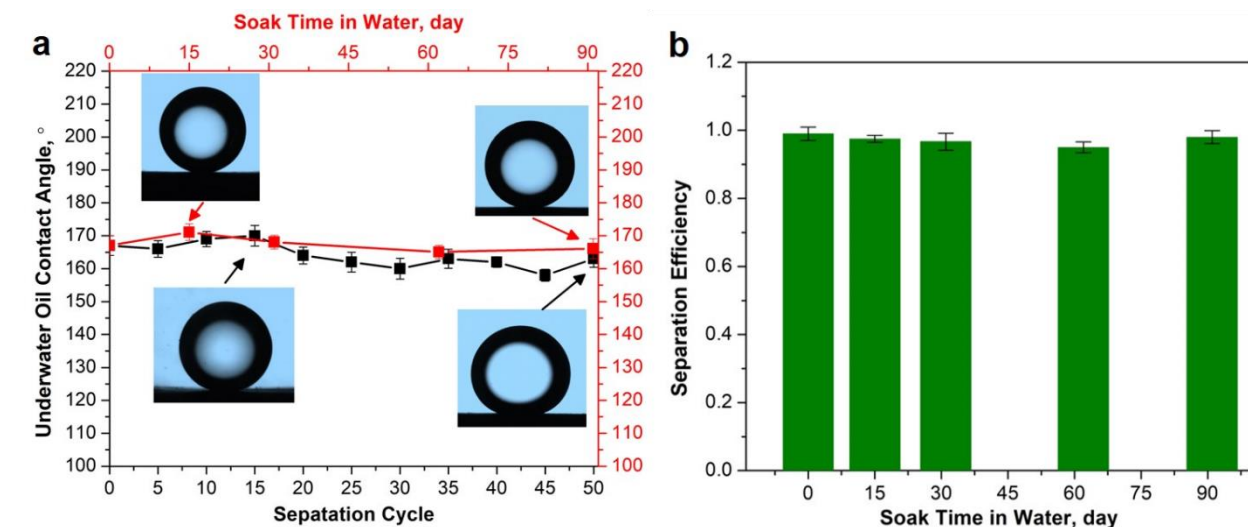Figure 9. (a) Underwater oil contact angle of d−UiO−66_2@mesh 400 monitored over the course of 3-month soaking in water and cyclic oil/water separation experiments and (b) oil rejection efficiency of water-soaked d−UiO−66_2@mesh-400s.

The stability of the oil/water separation performance of the d−UiO−66@mesh was first evaluated using a cyclic oil/water separation test. After each cycle of oil separation, the mesh was

flushed under running tap water for ~2 min and then dried at room temperature before underwater oil contact angle measurements. As displayed in Figure 9a, d−UiO−66_2@meshes 400 showed very stable underwater oil contact angle of about 158° even after 50 cycles of oil/water separation tests, revealing outstanding recyclability of the meshes (see also Table S5). To understand their capability in long-term oil separation, a similar 3-month water soaking test was conducted parallelly on multiple d−UiO−66_2@meshes 400. Their surface wettability and separation efficiency were monitored over the whole course of the soaking test. Figure 9a shows that the underwater superoleophobicity of the mesh surface was well preserved as the underwater oil contact angles remained greater than 160°, and Figure 9b shows the separation efficiency retained above 95% (see also Table S6 and Video S7), revealing outstanding long-term stability and oil rejection capability of the d−UiO−66_2@meshes 400. The mechanical stability of the d−UiO−66_2@meshes 400 was also tested by flushing the d−UiO−66 mesh surface directly under running water at a flow rate of 3.0 ± 0.65 L min^{-1} for 6 h. The SEM image of the mesh surface shows the d−UiO−66_2 coating layer was slightly cracked, but the underwater oil contact angle remained above 155° (Figure S4), indicating excellent mechanical stability. According to previous studies, UiO−66 and their defective analogues have excellent chemical stabilities (see "Chemical stabilities of UiO−66" in Supporting Information). However, more systematic studies on their hydrothermal stability under harsh conditions and oil/water separation at elevated temperatures which are representative and critical in many industrial processes (e.g., 35 °C ~ 85 °C, a normal temperature range found for industrial oily wastewaters) will be studied in the future.

CONCLUSIONS

We have tuned and studied the wettability of the UiO−66 via the engineering control over the defects inside its framework using modulation synthesis. UiO−66 crystals with tunable

hydrophilicity were prepared with a yield higher than 50%. A continuous dense layer of well-intergrown d−UiO−66 crystals was also successfully prepared on a series of stainless steel meshes using a two-step fabrication process. The synthesized d−UiO−66@meshes were superhydrophilic in air, superoleophobic in water and efficient in oil separation from various oil/water mixtures. Based on both cyclic separation tests and long-term stability tests, these d−UiO−66@meshes showed reusability and stability. The concept of fine-tuning the hydrophilicity of UiO−66 framework via defect engineering may be applicable to other MOFs which possess the capabilities of losing specific framework ligands but can still retain satisfactory stability. The results obtained in this work give new insights into the search for potential MOF-based materials for liquid separations and also for a wide range of interfacial-related applications.

ASSOCIATED CONTENT

Supporting Information

Supporting Information to this article can be found online at https://doi.org.

Density Functional Theory (DFT) Calculations, Molecular Simulations, Missing linker calculation, PXRD patterns of UiO−66 samples before and after 3 month water soaking, SEM images of d−UiO−66_2@mesh fabrication without PDA coating and with higher acid ratio in the precursor, and LJ parameters and atomic charge for H_2O can be found in supporting information.

AUTHOR INFORMATION

Corresponding Author

E-mail: krista.walton@chbe.gatech.edu.

Author Contributions

Y.H., Y.J., T.C., and Y.G. contributed equally. Y.H., Y.J., T.C., and Y.G. completed the experiments, Y.H. and T.C. wrote the manuscript. The manuscript was revised through contributions of all authors. All authors have given approval to the final version of the manuscript.

REFERENCES

(1)   Lu, G.; Li, S.; Guo, Z.; Farha, O. K.; Hauser, B. G.; Qi, X.; Wang, Y.; Wang, X.; Han, S.; Liu, X.; et al. Imparting Functionality to a Metal-Organic Framework Material by Controlled Nanoparticle Encapsulation. *Nat. Chem.* **2012**, *4*, 310–316.

(2)   Farha, O. K.; Yazaydin, A. Ö.; Eryazici, I.; Malliakas, C. D.; Hauser, B. G.; Kanatzidis, M. G.; Nguyen, S. T.; Snurr, R. Q.; Hupp, J. T. De Novo Synthesis of a Metal-Organic Framework Material Featuring Ultrahigh Surface Area and Gas Storage Capacities. *Nat. Chem.* **2010**, *2*, 944–948.

(3)   Zhou, H. C.; Long, J. R.; Yaghi, O. M. Introduction to Metal-Organic Frameworks. *Chem. Rev.* **2012**, *112*, 673–674.

(4)   Furukawa, H.; Cordova, K. E.; O'Keeffe, M.; Yaghi, O. M. The Chemistry and Applications of Metal-Organic Frameworks. *Science* **2013**, *341* (6149).

(5)   Li, B.; Chen, D.; Wang, J.; Yan, Z.; Jiang, L.; Duan, D.; He, J.; Luo, Z.; Zhang, J.; Yuan, F. MOFzyme: Intrinsic Protease-like Activity of Cu-MOF. *Sci. Rep.* **2014**, *4*, 39–43.

(6)   Fortea-Pérez, F. R.; Mon, M.; Ferrando-Soria, J.; Boronat, M.; Leyva-Pérez, A.; Corma, A.; Herrera, J. M.; Osadchii, D.; Gascon, J.; Armentano, D.; Pardo, E. The MOF-Driven Synthesis of Supported Palladium Clusters with Catalytic Activity for Carbene-Mediated Chemistry. *Nat. Mater.* **2017**, *16*, 760–766.

(7)   Hu, Y.; Wei, J.; Liang, Y.; Zhang, H.; Zhang, X.; Shen, W.; Wang, H. Zeolitic Imidazolate Framework/Graphene Oxide Hybrid Nanosheets as Seeds for the Growth of Ultrathin Molecular Sieving Membranes. *Angew. Chemie Int. Ed.* **2016**, *55*, 2048–2052.

(8)   Zhang, H.; Liu, X.; Wu, Y.; Guan, C.; Cheetham, A. K.; Wang, J. MOF-Derived Nanohybrids for Electrocatalysis and Energy Storage: Current Status and Perspectives. *Chem. Commun.* **2018**, *54*, 5268–5288.

(9)   Sholl, D. S.; Lively, R. P. Defects in Metal-Organic Frameworks: Challenge or Opportunity? *J. Phys. Chem. Lett.* **2015**, *6*, 3437–3444.

(10)   Fang, Z.; Bueken, B.; De Vos, D. E.; Fischer, R. A. Defect-Engineered Metal-Organic Frameworks. *Angew. Chemie - Int. Ed.* **2015**, *54*, 7234–7254.

(11)   Furukawa, H.; Müller, U.; Yaghi, O. M. "Heterogeneity within Order" in Metal-Organic Frameworks. *Angew. Chemie - Int. Ed.* **2015**, *54*, 3417–3430.

(12)   Nasalevich, M. A.; Hendon, C. H.; Santaclara, J. G.; Svane, K.; Van Der Linden, B.; Veber, S. L.; Fedin, M. V.; Houtepen, A. J.; Van Der Veen, M. A.; Kapteijn, F.; Walsh, A.; Gascon, J.

Electronic Origins of Photocatalytic Activity in D0 Metal-Organic Frameworks. *Sci. Rep.* **2016**, *6*, 1–9.

(13) Song, Z.; Liu, W.; Cheng, N.; Norouzi Banis, M.; Li, X.; Sun, Q.; Xiao, B.; Liu, Y.; Lushington, A.; Li, R.; Liu, L; Sun, X. Origin of the High Oxygen Reduction Reaction of Nitrogen and Sulfur Co-Doped MOF-Derived Nanocarbon Electrocatalysts. *Mater. Horizons* **2017**, *4*, 900–907.

(14) Vermoortele, F.; Vandichel, M.; Van De Voorde, B.; Ameloot, R.; Waroquier, M.; Van Speybroeck, V.; De Vos, D. E. Electronic Effects of Linker Substitution on Lewis Acid Catalysis with Metal-Organic Frameworks. *Angew. Chemie Int. Ed.* **2012**, *51*, 4887–4890.

(15) Liang, W.; Li, L.; Hou, J.; Shepherd, N. D.; Bennett, T. D.; D'Alessandro, D. M.; Chen, V. Linking Defects, Hierarchical Porosity Generation and Desalination Performance in Metal-Organic Frameworks. *Chem. Sci.* **2018**, *9*, 3508–3516.

(16) Wang, K.; Li, C.; Liang, Y.; Han, T.; Huang, H.; Yang, Q.; Liu, D.; Zhong, C. Rational Construction of Defects in a Metal-Organic Framework for Highly Efficient Adsorption and Separation of Dyes. *Chem. Eng. J.* **2016**, *289*, 486–493.

(17) Li, B.; Zhu, X.; Hu, K.; Li, Y.; Feng, J.; Shi, J.; Gu, J. Defect Creation in Metal-Organic Frameworks for Rapid and Controllable Decontamination of Roxarsone from Aqueous Solution. *J. Hazard. Mater.* **2016**, *302*, 57–64.

(18) DeCoste, J. B.; Demasky, T. J.; Katz, M. J.; Farha, O. K.; Hupp, J. T. A UiO−66 Analogue with Uncoordinated Carboxylic Acids for the Broad-Spectrum Removal of Toxic Chemicals. *New J. Chem.* **2015**, *39*, 2396–2399.

(19)   Ghosh, P.; Colón, Y. J.; Snurr, R. Q. Water Adsorption in UiO−66: The Importance of Defects. *Chem. Commun.* **2014**, *50*, 11329–11331.

(20)   Thornton, A. W.; Babarao, R.; Jain, A.; Trousselet, F.; Coudert, F. X. Defects in Metal-Organic Frameworks: A Compromise between Adsorption and Stability? *Dalt. Trans.* **2016**, *45*, 4352–4359.

(21)   Vermoortele, F.; Bueken, B.; Le Bars, G.; Van De Voorde, B.; Vandichel, M.; Houthoofd, K.; Vimont, A.; Daturi, M.; Waroquier, M.; Van Speybroeck, V.; Kirschhock, C.; De Vos, D. E. Synthesis Modulation as a Tool to Increase the Catalytic Activity of Metal-Organic Frameworks: The Unique Case of UiO−66(Zr). *J. Am. Chem. Soc.* **2013**, *135*, 11465–11468.

(22)   Vermoortele, F.; Ameloot, R.; Alaerts, L.; Matthessen, R.; Carlier, B.; Fernandez, E. V. R.; Gascon, J.; Kapteijn, F.; De Vos, D. E. Tuning the Catalytic Performance of Metal-Organic Frameworks in Fine Chemistry by Active Site Engineering. *J. Mater. Chem.* **2012**, *22*, 10313–10321.

(23)   Park, T. H.; Hickman, A. J.; Koh, K.; Martin, S.; Wong-Foy, A. G.; Sanford, M. S.; Matzger, A. J. Highly Dispersed Palladium(II) in a Defective Metal-Organic Framework: Application to C-H Activation and Functionalization. *J. Am. Chem. Soc.* **2011**, *133*, 20138–20141.

(24)   Henke, S.; Schneemann, A.; Wütscher, A.; Fischer, R. A. Directing the Breathing Behavior of Pillared-Layered Metal-Organic Frameworks via a Systematic Library of Functionalized Linkers Bearing Flexible Substituents. *J. Am. Chem. Soc.* **2012**, *134*, 9464–9474.

(25)   Umemura, A.; Diring, S.; Furukawa, S.; Uehara, H.; Tsuruoka, T.; Kitagawa, S. Morphology Design of Porous Coordination Polymer Crystals by Coordination Modulation. *J. Am. Chem. Soc.* **2011**, *133*, 15506–15513.

(26)   Shearer, G. C.; Chavan, S.; Bordiga, S.; Svelle, S.; Olsbye, U.; Lillerud, K. P. Defect Engineering: Tuning the Porosity and Composition of the Metal-Organic Framework UiO−66 via Modulated Synthesis. *Chem. Mater.* **2016**, *28*, 3749–3761.

(27)   Schaate, A.; Roy, P.; Godt, A.; Lippke, J.; Waltz, F.; Wiebcke, M.; Behrens, P. Modulated Synthesis of Zr-Based Metal-Organic Frameworks: From Nano to Single Crystals. *Chem. A Eur. J.* **2011**, *17*, 6643–6651.

(28)   Van De Voorde, B.; Stassen, I.; Bueken, B.; Vermoortele, F.; De Vos, D.; Ameloot, R.; Tan, J. C.; Bennett, T. D. Improving the Mechanical Stability of Zirconium-Based Metal-Organic Frameworks by Incorporation of Acidic Modulators. *J. Mater. Chem. A* **2015**, *3*, 1737–1742.

(29)   Park, J.; Wang, Z. U.; Sun, L. B.; Chen, Y. P.; Zhou, H. C. Introduction of Functionalized Mesopores to Metal-Organic Frameworks via Metal-Ligand-Fragment Coassembly. *J. Am. Chem. Soc.* **2012**, *134*, 20110–20116.

(30)   Katz, M. J.; Klet, R. C.; Moon, S. Y.; Mondloch, J. E.; Hupp, J. T.; Farha, O. K. One Step Backward Is Two Steps Forward: Enhancing the Hydrolysis Rate of UiO−66 by Decreasing [OH-]. *ACS Catal.* **2015**, *5*, 4637–4642.

(31)   Wu, H.; Chua, Y. S.; Krungleviciute, V.; Tyagi, M.; Chen, P.; Yildirim, T.; Zhou, W. Unusual and Highly Tunable Missing-Linker Defects in Zirconium Metal-Organic Framework

UiO−66 and Their Important Effects on Gas Adsorption. *J. Am. Chem. Soc.* **2013**, *135*, 10525–10532.

(32)   Bueken, B.; Reinsch, H.; Reimer, N.; Stassen, I.; Vermoortele, F.; Ameloot, R.; Stock, N.; Kirschhock, C. E. A.; De Vos, D. A Zirconium Squarate Metal-Organic Framework with Modulator-Dependent Molecular Sieving Properties. *Chem. Commun.* **2014**, *50*, 10055–10058.

(33)   Shannon, M. A.; Bohn, P. W.; Elimelech, M.; Georgiadis, J. G.; Marĩas, B. J.; Mayes, A. M. Science and Technology for Water Purification in the Coming Decades. *Nature* **2008**, *452*, 301–310.

(34)   Jamaly, S.; Giwa, A.; Hasan, S. W. Recent Improvements in Oily Wastewater Treatment: Progress, Challenges, and Future Opportunities. *J. Environ. Sci.* **2015**, *37*, 15–30.

(35)   Wang, B.; Liang, W.; Guo, Z.; Liu, W. Biomimetic Super-Lyophobic and Super-Lyophilic Materials Applied for Oil/Water Separation: A New Strategy beyond Nature. *Chem. Soc. Rev.* **2015**, *44*, 336–361.

(36)   Xue, Z.; Cao, Y.; Liu, N.; Feng, L.; Jiang, L. Special Wettable Materials for Oil/Water Separation. *J. Mater. Chem. A* **2014**, *2*, 2445–2460.

(37)   Huang, Y.; Li, H.; Wang, L.; Qiao, Y.; Tang, C.; Jung, C.; Yoon, Y.; Li, S.; Yu, M. Ultrafiltration Membranes with Structure-Optimized Graphene-Oxide Coatings for Antifouling Oil/Water Separation. *Adv. Mater. Interfaces* **2015**, *2*, 1400433

(38)   Meng, X.; Wang, M.; Heng, L.; Jiang, L. Underwater Mechanically Robust Oil-Repellent Materials: Combining Conflicting Properties Using a Heterostructure. *Adv. Mater.* **2018**, *30*, 1–8.

(39)   Dong, Y.; Li, J.; Shi, L.; Wang, X.; Guo, Z.; Liu, W. Underwater Superoleophobic Graphene Oxide Coated Meshes for the Separation of Oil and Water. *Chem. Commun.* **2014**, *50*, 5586–5589.

(40)   Liu, Y. Q.; Zhang, Y. L.; Fu, X. Y.; Sun, H. B. Bioinspired Underwater Superoleophobic Membrane Based on a Graphene Oxide Coated Wire Mesh for Efficient Oil/Water Separation. *ACS Appl. Mater. Interfaces* **2015**, *7*, 20930–20936.

(41)   Yuan, L.; Tian, M.; Lan, J.; Cao, X.; Wang, X.; Chai, Z.; Gibson, J. K.; Shi, W. Defect Engineering in Metal-Organic Frameworks: A New Strategy to Develop Applicable Actinide Sorbents. *Chem. Commun.* **2018**, *54*, 370–373.

(42)   Cavka, J. H.; Jakobsen, S.; Olsbye, U.; Guillou, N.; Lamberti, C.; Bordiga, S.; Lillerud, K. P. A New Zirconium Inorganic Building Brick Forming Metal Organic Frameworks with Exceptional Stability. *J. Am. Chem. Soc.* **2008**, *130*, 13850–13851.

(43)   DeStefano, M. R.; Islamoglu, T.; Garibay, S. J.; Hupp, J. T.; Farha, O. K. Room-Temperature Synthesis of UiO−66 and Thermal Modulation of Densities of Defect Sites. *Chem. Mater.* **2017**, *29*, 1357–1361.

(44)   Lee, H.; Dellatore, S. M.; Miller, W. M.; Messersmith, P. B. Mussel-inspired surface chemistry for multifunctional coatings. *Science* **2007**, 318, 426-430.

(45)   Liu, X.; Demir, N. K.; Wu, Z.; Li, K. Highly Water-Stable Zirconium Metal-Organic Framework UiO−66 Membranes Supported on Alumina Hollow Fibers for Desalination. *J. Am. Chem. Soc.* **2015**, *137*, 6999–7002.

(46)   Klet, R. C.; Liu, Y.; Wang, T. C.; Hupp, J. T.; Farha, O. K. Evaluation of Brønsted Acidity and Proton Topology in Zr- and Hf-Based Metal-Organic Frameworks Using Potentiometric Acid-Base Titration. *J. Mater. Chem. A.* **2016**, *4*, 1479–1485.

(47)   Agrawal, M.; Han, R.; Herath, D.; Sholl, D. S. Does Repeat Synthesis in Materials Chemistry Obey a Power Law? *Proc. Natl. Acad. Sci. U. S. A.* **2020**, *117*, 877–882.

Table of Contents

Defect UiO-66 mesh film for oil/water mixture separation

Oil/water mixture

Water

C
Zr
H
O
Defects

Defect engineered UiO-66 with enhanced hydrophilicity and underwater superoleophobicity